



Review

# Dielectric-Based Rear Surface Passivation Approaches for Cu(In,Ga)Se<sub>2</sub> Solar Cells—A Review

Gizem Birant<sup>1,2,3,\*</sup> , Jessica de Wild<sup>1,2,3</sup>, Marc Meuris<sup>1,2,3</sup>, Jef Poortmans<sup>3,4,5</sup> and Bart Vermang<sup>1,2,3</sup> 

<sup>1</sup> Institute for Material Research (IMO), Hasselt University, Agoralaan gebouw H, 3590 Diepenbeek, Belgium; Jessica.deWild@imec.be (J.d.W.); Marc.Meuris@imec.be (M.M.); bart.vermang@imec.be (B.V.)

<sup>2</sup> Imec division IMOMECA (partner in Solliance), Wetenschapspark 1, 3590 Diepenbeek, Belgium

<sup>3</sup> Energyville, Thor Park 8320, 3600 Genk, Belgium; Jef.Poortmans@imec.be

<sup>4</sup> imec (partner in Solliance), Kapeldreef 75, 3001 Leuven, Belgium

<sup>5</sup> Department of Electrical Engineering, KU Leuven, Kasteelpark Arenberg 10, 3001 Heverlee, Belgium

\* Correspondence: gizem.birant@imec.be

Received: 14 January 2019; Accepted: 12 February 2019; Published: 16 February 2019



**Abstract:** This review summarizes all studies which used dielectric-based materials as a passivation layer at the rear surface of copper indium gallium (di)selenide, Cu(In,Ga)Se<sub>2</sub>, (CIGS)-based thin film solar cells, up to 2019. The results regarding the kind of dielectric materials, the deposition techniques, contacting approaches, the existence of additional treatments, and current–voltage characteristics (J–V) of passivated devices are emphasized by a detailed table. The techniques used to implement the passivation layer, the contacting approach for the realization of the current flow between rear contact and absorber layer, additional light management techniques if applicable, the solar simulator results, and further characterization techniques, i.e., external quantum efficiency (EQE) and photoluminescence (PL), are shared and discussed. Three graphs show the difference between the reference and passivated devices in terms of open-circuit voltage ( $V_{oc}$ ), short-circuit current ( $J_{sc}$ ), and efficiency ( $\eta$ ), with respect to the thicknesses of the absorber layer. The effects of the passivation layer at the rear surface are discussed based on these three graphs. Furthermore, an additional section is dedicated to the theoretical aspects of the passivation mechanism.

**Keywords:** CIGS; solar cells; review; passivation

## 1. Introduction

The energy coming from the sun has the highest potential energy of all renewable resources, and it is ~35,000 times higher than today's energy needs on a yearly basis. Semiconductor-based technologies, i.e., photovoltaic (PV) technologies, are developed to convert this energy into electrical energy. Today, the dominant market share (95%) belongs to Silicon (Si) PV technologies [1]. However, considering the weight, rigidity, and processing restrictions of Si PV, alternative materials and technologies have been sought and developed over the years [2]. Thin film (TF) PV technology is an outcome of these researches, and among all TF PV technologies, Cu(In, Ga)Se<sub>2</sub> (CIGS)-based solar cells have the highest cell and module efficiencies [3].

The basic structure of CIGS solar cells is given in Figure 1. The production step starts with a sputtering molybdenum (Mo) layer as an electrical back contact on soda-lime glass (SLG), metal, or polymer substrate. It is continued with the p-type CIGS absorber layer deposition by using co-evaporation, sputtering, or electro-deposition techniques. During the CIGS deposition, due to the formation of a MoSe<sub>2</sub> layer, quasi-ohmic contact between the CIGS and the Mo layer is facilitated [2]. The production process of a CIGS solar cell continues with the deposition of the

n-type buffer layer, generally cadmium sulfide (CdS). This process is completed with deposition of a transparent conducting oxide (TCO) window layer. In order to increase the efficiency, in some studies, an anti-reflection coating layer is also applied as a final touch [4].

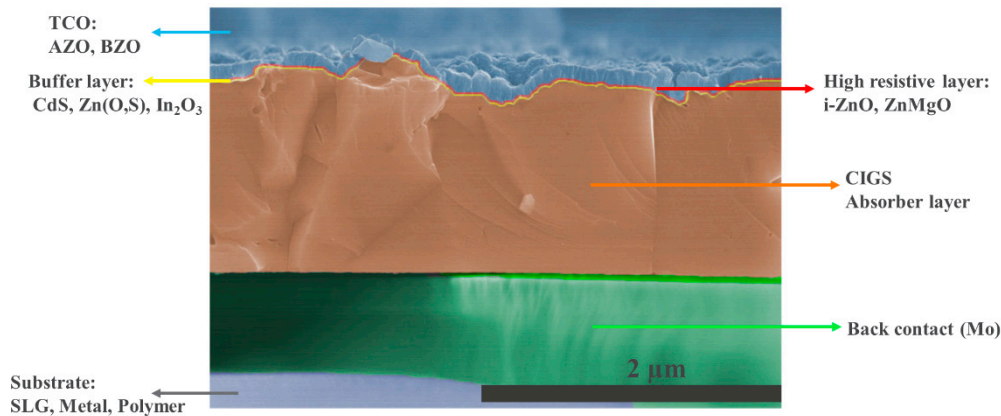


**Figure 1.** Detailed structure of conventional Cu(In,Ga)Se<sub>2</sub> (CIGS) solar cell with examples of the most commonly used materials, adapted from [4].

As mentioned earlier, the biggest competitor of the CIGS solar cells is Si PV technology. In order to compete with high-efficiency and low-cost Si PV, the power conversion efficiency of CIGS solar cells should be increased, and the thickness of the absorber layer should be decreased [1]. Considering the fact that In and Ga are critical raw materials, reducing the thickness of the absorber layer has another positive outcome: decreasing the amount of In and Ga used. However, decreasing the thickness of the absorber layer causes insufficient absorption and the detrimental impact of back-surface recombination [5]. Consequently, the power conversion efficiency of the thin CIGS-based solar cells decreases. If the thickness of the absorber layer is decreased, the electrical quality of these solar cells, hence, the power conversion efficiency, should be kept the same or, if possible, improved.

The traditional way to enhance the electrical quality of the CIGS solar cell is gallium (Ga) grading. For thick absorber layers, the Ga gradient is in the neutral region of the absorber layer and creates a back surface field (BSF). If the absorber layers are thinner, they become completely depleted, and the BSF is created in the space charge region (SCR), improving  $V_{oc}$  for thin absorber layers [6]. Ga grading is not a complete solution for passivation of the rear surface because an additional counteract electric field (E-field) occurs, which causes an overall weaker E-field in SCR [6]. Consequently, a new and improved solution to passivate the rear surface of CIGS solar cells was sought. Introducing a passivation layer with point openings that ensures electrical contact between the rear contact and the absorber layer is one of the solutions to this problem (Figure 2). In this paper, an overview of the papers that use this approach for rear surface passivation of CIGS solar cells to date is given.

## 2. Theoretical Aspects

As the creation of electron–hole pairs via photons is the fundamental principal of PV technology, the opposite mechanism, i.e., recombination, can cause a reduction in voltage ( $V_{oc}$ ). If the following formula (1) is examined, the effects of the recombination mechanism on  $V_{oc}$  can be seen [7],

$$V_{oc} = \frac{nkT}{q} \ln\left(\frac{I_L}{I_0} + 1\right) \quad (1)$$

where  $n$  is the ideality factor,  $kT/q$  is the thermal voltage,  $I_L$  is the light generated current, and  $I_0$  is the saturation current, which depends on the recombination velocities [7]. The rate of the surface

recombination ( $U_s$ ), on the other hand, can be expressed as a function of interface defect density,  $N_{it}$  [8]. Its description is derived from the Shockley-Read-Hall (SRH) formalism:

$$U_s = \frac{(n_s p_s - n_i^2) v_{th} N_{it}}{\frac{n_s + n_1}{\sigma_p} + \frac{p_s + p_1}{\sigma_n}} \quad (2)$$

where  $\sigma_{p/n}$  is the hole and electron capture cross section,  $p_s$  and  $n_s$  are the hole and electron densities,  $v_{th}$  is the thermal velocity of the electrons,  $n_1$  and  $p_1$  are statistical factors, and  $n_i$  is the intrinsic carrier concentration [8]. Slight variations in the CIGS structure and bond angle cause surface defects, and therefore, formula (2) should be corrected. Changing the  $N_{it}$  term to the  $D_{it}$  (interface trap density) at the extended SRH formalism with an integral over the bandgap energies is a way to correct the formula (2) [8].

If formula (2) is taken into consideration, it can be clearly seen that reducing  $U_s$  is possible by introducing a passivation layer. Two possible mechanisms will occur due to the implementation of this layer; these are chemical passivation and field-effect passivation. The total number of electrically active defects, i.e., dangling bonds, is decreased after the addition of the passivation layer. It is called the chemical passivation [9]. An implemented passivation layer, which has a high density of fixed charges ( $Q_f$ ), repels the minority carriers, i.e., reduces  $U_s$ , by creating an electric field [10]. It is called field-effect passivation. Besides the reduction of the recombination rate, the dielectric layer also increases reflection at the rear surface for certain thicknesses [11]. In this way, the optical path length of the light is increased.

### 3. Dielectric-Based Passivation Layers

The overview of the studies using a dielectric material as the rear surface passivation layer for CIGS solar cells to date is given in the Table 1. This table introduces the type of the material that is used for passivation and the deposition techniques used for these layers as well as the required contacting approaches and the thickness of the absorber layer. The light management techniques, anti-reflection coating (ARC) layer applications, additional sodium (Na) supply, and gallium (Ga) grading are also given in this table. If any of these four approaches are applied or not applied in a given study, it is indicated with a plus sign (+) or with a minus sign (-), respectively. Table 1 also gives the average JV results of the devices that have a passivation layer.

**Table 1.** Overview of the studies about rear surface passivation of CIGS solar cells up to 2019, including the dielectric layers, deposition techniques of these layers, contacting approaches, additional light management strategies, anti-reflection coating (ARC) application, additional Na supply, Ga grading, thicknesses of the absorber layers ( $t_{\text{CIGS}}$ ), and average solar simulator results of rear passivated solar cells.

Dielectric and Its Thickness	Deposition Technique	Contacting Approach	Light Management	ARC	Na Supply	Ga Grading	$t_{\text{CIGS}}$ ( $\mu\text{m}$ )	Average		
								$V_{oc}$ (mV)	$J_{sc}$ (mA/cm <sup>2</sup> )	FF (%)
Al <sub>2</sub> O <sub>3</sub> -18 nm [9]	ALD	e-beam lithography	-	-	+	+	0.35	627 ± 11	21.56 ± 1	71.8 ± 3.3
Al <sub>2</sub> O <sub>3</sub> -2 nm [12]	ALD	CBD of CdS NPs	-	-	+	+	1.50	638 ± 3	30 ± 0.6	78.8 ± 0.3
Al <sub>2</sub> O <sub>3</sub> -5 nm [13]	ALD	CBD of CdS NPs	-	-	+	+	0.48	650 ± 5	22 ± 1	-
Al <sub>2</sub> O <sub>3</sub> -5 nm [13]	ALD	CBD of CdS NPs	-	-	+	+	1.58	635 ± 5	30 ± 1	78.8
Al <sub>2</sub> O <sub>3</sub> -25 nm [14]	DC Sputtering	CBD of CdS NPs	-	+	+	-	0.4	624 ± 2	29 ± 0.4	72.6 ± 0.5
Al <sub>2</sub> O <sub>3</sub> -50 nm [14]	DC Sputtering	CBD of CdS NPs	-	+	+	-	0.4	644 ± 6	30.2 ± 0.8	67.8 ± 1.7
Al <sub>2</sub> O <sub>3</sub> -5 nm [14]	ALD	CBD of CdS NPs	MgF <sub>2</sub>	+	+	-	0.4	633 ± 2	31.1 ± 0.1	68.7 ± 1.9
Al <sub>2</sub> O <sub>3</sub> -(10/15) nm [15]	DC Sputtering	(HIPP) Mo NPs	Mo NPs *	-	+	-	0.35	508 ± 39	22.1 ± 0.4	57 ± 3
Al <sub>2</sub> O <sub>3</sub> -(10/15) nm [15]	DC Sputtering	(HIPP) Mo NPs	Mo NPs *	+	+	+	0.38	530 ± 31	25.7 ± 0.4	65 ± 2
Al <sub>2</sub> O <sub>3</sub> -5 nm [16]	ALD	Photo-lithography	-	+	-	-	1.89	737 ± 22	32.3 ± 1.6	76.6 ± 0.9
Al <sub>2</sub> O <sub>3</sub> -5 nm [16]	ALD	Photo-lithography	-	+	-	-	0.38	644 ± 22	23.8 ± 2.1	66.7 ± 1.5
Al <sub>2</sub> O <sub>3</sub> - 27 nm [17]	ALD	e-beam lithography	-	-	+	+	0.60	732 ± 3	18.8 ± 0.4	68 ± 3
Al <sub>2</sub> O <sub>3</sub> - 27 nm [17]	ALD	e-beam lithography	-	-	+	+	0.85	721 ± 10	20 ± 0.2	69 ± 0
Al <sub>2</sub> O <sub>3</sub> - 27 nm [17]	ALD	e-beam lithography	-	-	+	+	1.45	747 ± 4	22.9 ± 0.7	70 ± 1
Al <sub>2</sub> O <sub>3</sub> -10 nm [18]	-	e-beam lithography	-	+	+	-	0.24	659 ± 5	23.3 ± 0.5	77.0 ± 0.6
Al <sub>2</sub> O <sub>3</sub> -25 nm ** [11]	ALD	Photo-lithography	-	-	-	+	0.5	547 ± 4	24.6 ± 0.2	68 ± 2
Al <sub>2</sub> O <sub>3</sub> -50 nm ** [11]	ALD	Photo-lithography	-	-	-	+	0.5	550 ± 1	24.6 ± 0	68 ± 1
MgF <sub>2</sub> -100 nm ** [11]	Thermal evaporation	Photo-lithography	MgF <sub>2</sub> *	-	-	+	0.5	562 ± 3	24.8 ± 0.2	71 ± 0
SiO <sub>2</sub> NPs *** [19]	Spin coating	SCIL	-	+	-	+	0.39	533 ± 3	30.5 ± 0.2	53.9 ± 2.0
SiO <sub>2</sub> NPs *** [19]	Spin coating	SCIL	Ag Mirror	+	-	+	0.39	558 ± 2	32.4 ± 0.2	55.2 ± 1.7

Table 1. Cont.

Dielectric and Its Thickness	Deposition Technique	Contacting Approach	Light Management	ARC	Na Supply	Ga Grading	$t_{\text{CIGS}}$ ( $\mu\text{m}$ )	Average		
								$V_{oc}$ (mV)	$J_{sc}$ (mA/cm <sup>2</sup> )	FF (%)
Al <sub>2</sub> O <sub>3</sub> -15 nm [5]	ALD	Nano-imprint lithography	-	-	-	-	0.40	458	23.6	53
TiO <sub>2</sub> -50 nm [5]	Spin coating	Nano-imprint lithography	-	-	-	-	0.40	422	19.3	53
Al <sub>2</sub> O <sub>3</sub> -15 nm [5]	ALD	Nano-imprint lithography	-	-	+	-	0.42	604	20.9	73
TiO <sub>2</sub> -50 nm [5]	Spin coating	Nano-imprint lithography	-	-	+	-	0.42	606	19.5	63
SiO <sub>2</sub> -NPs [20]	e-beam evaporation	SCIL	SiO <sub>2</sub> NPs *	-	-	+	0.46	592	30.6	68.2
Al <sub>2</sub> O <sub>3</sub> **** [21]	ALD	CBD of CdS NPs	-	-	+	-	0.40	644 ± 6	28.4 ± 0.2	67.8 ± 1.7
SiO <sub>2</sub> NM [22]	Thermal evaporation	Nano-sphere lithography	SiO <sub>2</sub> NPs *	-	-	+	0.37	589	27.5	70.3
SiO <sub>2</sub> -25 nm ***** [23]	CVD	Photo-lithography	-	-	+	+	0.45	607 ± 5	18.2 ± 0.3	52.2 ± 8.9
Al <sub>2</sub> O <sub>3</sub> -6.3 nm [24]	ALD	Tunneling	-	-	+	+	1	555	34	70
Al <sub>2</sub> O <sub>3</sub> -7 nm [25]	ALD	CBD of CdS NPs	-	-	+	-	0.43	597 ± 7	22.9 ± 0.3	62.1 ± 2
Al <sub>2</sub> O <sub>3</sub> -7 nm [25]	ALD	CBD of CdS NPs	Ag NPs	-	+	-	0.43	560 ± 7	23.3 ± 0.3	60.1 ± 0.6

\* passivation layer/NPs also act as light management technique. \*\* periodicity of the openings chosen as 6  $\mu\text{m}$  with 3  $\mu\text{m}$  wide contact area. \*\*\* back contact is indium tin oxide (ITO). \*\*\*\* after recovery of potential induced degradation for Na diffusion. \*\*\*\*\* line width chosen as 0.7  $\mu\text{m}$  and pitch chosen as 2  $\mu\text{m}$ .

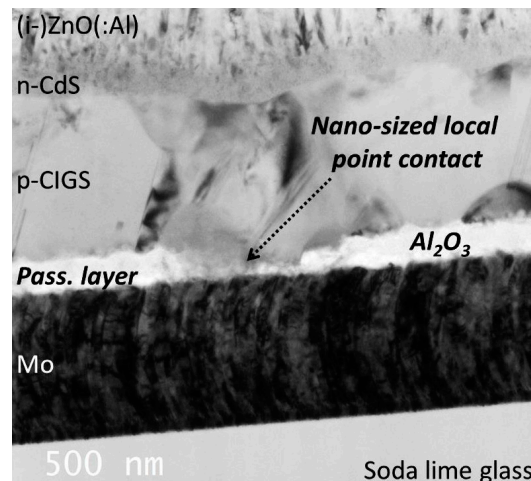


**Figure 2.** Transmission electron microscopy (TEM) image of  $\text{Al}_2\text{O}_3$ -passivated CIGS solar cell that has nano-sized local point contacts in passivation layer [14].

After the creation of the passivation layer, the thickness of this layer was determined using high angle annular dark-field (HAADF) transmission electron microscopy (TEM) in [9], spectrally resolved ellipsometry in [12,13,16,17,24,25], TEM in [14,18], energy dispersive X-ray spectroscopy (EDX) in [15], scanning electron microscopy (SEM) in [11,19,20,22], profilometry in [5], and atomic force microscopy (AFM) in [23]. The thickness of the passivation layer should be chosen to be sufficiently thin ( $\sim 1\text{--}2$  nm) to allow tunneling if there is no contact opening approach applied to this layer.

In the following subsections, (3.1) approaches used to add the passivation layer, (3.2) contacting approaches, (3.3) light management techniques, (3.4) solar simulator results, and (3.5) other characterization techniques used for further analyses will be discussed.

### 3.1. Approaches Used to Add the Passivation Layer

In this sub-section, the type of materials that are used as passivation layers and the deposition techniques of these layers will be discussed. As shown in Table 1, in most of the studies, aluminum oxide ( $\text{Al}_2\text{O}_3$ ) was used as a passivation layer. The popularity of this material comes from the Si PV community.  $\text{Al}_2\text{O}_3$  is commonly used and is proven to be a successful passivation layer for Si solar cells in many studies like [26].  $\text{Al}_2\text{O}_3$  is also proven to be functional as a passivation layer for CIGS solar cells by reducing recombination losses at the rear metal contact of CIGS thin-film solar cells [27]. Unfortunately, it also acts as an electron and diffusion barrier layer, and thus prevents current flow and sodium (Na) diffusion from the SLG substrate. To trick the natural behavior of alumina layers, i.e., insulator (or barrier) layer, different techniques are used to make contact openings in this layer, which will be discussed in the following section.

In the studies that did not use  $\text{Al}_2\text{O}_3$  as a passivation layer, silicon ( $\text{SiO}_2$ ) nanoparticles (NPs) or nano-meshes (NM), magnesium fluoride ( $\text{MgF}_2$ ) layers, or titanium oxide ( $\text{TiO}_2$ ) layers were implemented with various techniques to act as a passivation layer in combination with contact opening approaches (Table 1). Using  $\text{SiO}_2$  NPs [19],  $\text{SiO}_2$  NM [22], and  $\text{MgF}_2$  [11] as passivation layers was successful. However, using  $\text{TiO}_2$  as a passivation layer caused a reduction in  $V_{oc}$ , fill factor (FF), and efficiency [5]. Hence, it was not a sufficient passivation layer yet.

Furthermore, in some of these studies, additional Na supply (only important for the studies using SLG as substrates), Ga grading, or additional light management techniques were used (Table 1).

In order to deposit the passivation layers, various techniques were used, such as atomic layer deposition (ALD), direct current (DC) sputtering, thermal evaporation, spin coating, e-beam evaporation, and chemical vapor deposition (CVD). The most commonly used technique is ALD. There are many advantages of ALD, such as creating a conformal layer with easily controllable layer

thickness and a variety of materials that can be used. Spin coating is another easy and fast technique to create the passivation layer, yet this technique is not applicable to large scale materials. There is also a more technologically viable technique to create these layers, which is DC sputtering. DC sputtering is a highly versatile vacuum coating system used for the deposition of a variety of materials at any preferred scale, i.e., a technologically viable way.

Among all other studies that used  $\text{Al}_2\text{O}_3$  as a passivation layer, only one study used this passivation layer alone, without using an additional contacting approach. In that study, it was proposed that using a very thin layer of  $\text{Al}_2\text{O}_3$  rear surface passivation in combination with NaF deposition enhances the electrical characteristics of CIGS solar cells. In that study this surface passivation was claimed to allow tunneling [24] (Table 1).

In order to investigate the effects and influence of back surface passivation in CIGS solar cells, there are studies that used bi-facial thin CIGS solar cells [28–30]. For bi-facial solar cells, all characterizations are made from both the front and back side of the solar cell. In [30], atomic-layer-deposited  $\text{Al}_2\text{O}_3$  was used for surface passivation, and lift-off processed CdS NPs were used to create nano-sized contact openings in this layer. At the end of this study, it was concluded that passivated solar cells gave a higher external quantum efficiency (EQE) response, both when measured from the front and from the rear side, and there was a minor improvement in  $V_{oc}$  values.

### 3.2. Contacting Approach

In this sub-section, several contacting approach techniques which are mentioned in Table 1 will be discussed for the  $\text{Al}_2\text{O}_3$  passivation layers. Due to the short diffusion length of CIGS carriers, the dimensions of the openings and the distance between them should be in the sub-micron range [9].

In the following studies [12–14,21,25], the contact openings were realized by chemical bath deposition (CBD) of CdS. The size, shape, and density of these particles are determined by the CBD parameters. The alumina layer is deposited on top of the particles. The CdS particles are then removed, leaving holes behind in the alumina layer. As the characteristics and morphologies of the particles are different from each other for the different studies, the outcomes of these studies are also different in terms of the effects on and/or enhancements of the electrical characteristics of the solar cells (Table 1).

Mo NPs generated by highly ionized pulsed plasma (HIPP) were also used as contacts in the  $\text{Al}_2\text{O}_3$  passivation layer. Here, the alumina was deposited by DC sputtering. Because of the one-directional growth of the alumina layer, the Mo nanoparticles were not completely covered with alumina, leaving space for contacting. Although there is a minor improvement in power conversion efficiency of the ultra-thin CIGS solar cells, this approach is still open to optimization [15] (Table 1).

To generate the contact openings in the  $\text{Al}_2\text{O}_3$  passivation layer, advanced techniques such as e-beam, nano-imprint, nano-sphere, or photolithography were used in the following studies [5,9,11,16–18,22,23]. Lithography is one of the most advanced techniques that is used for this purpose. It has advantages like creating the holes in a controlled shape, size, and density. However, it is an expensive technique for using it as an industrially viable technology. Using passivation layers with advanced opening techniques, i.e., lithography, results in improvements in electrical characteristics of both ultrathin and conventional CIGS solar cells (Table 1). In [11], different from the other studies,  $\text{MgF}_2$  (100nm) was used as a passivation layer together with  $\text{Al}_2\text{O}_3$  and resulted in significant optical improvement due to enhanced reflectivity at the back contact.

Using dielectric nanoparticles between back contact and absorber layer is another approach for the rear surface passivation of CIGS solar cells. In [19] and [20], the dielectric patterns were applied by the technique described in [19] to passivate the back surface but at the same time allow current to pass between the rear contact and the absorber layers. Hence, the geometrical requirements to have a good electrical contact were satisfied in these studies [12].

Ultimately, one of the different techniques explained above can be a suitable strategy to use for contacting. It is only necessary to decide the length and the cost of the experiment before choosing the strategy.

### 3.3. Light Management Techniques at Back Contact

Light management in photovoltaic devices means giving the light another chance to be absorbed inside the solar cell, i.e., increasing the optical path length of the light. As mentioned in the previous section, using NPs is a convenient solution to manage the path of the light inside the solar cell by changing the direction of the light by reflection. The effect of the light management can clearly be seen in external quantum efficiency (EQE) and/or absorption measurements of the devices, which will be discussed in section v.

Another way to control the incoming light at the rear surface is to use an additional silver (Ag) back mirror or Ag NPs at the rear surface under the passivation layer. In [19], Sn:In<sub>2</sub>O<sub>3</sub>, indium tin oxide (ITO), was used as a back contact instead of Mo. ITO allows the use of a mirror on the glass substrate, different than Mo rear contact. In [19], SiO<sub>2</sub> NPs were used as a passivation layer and an Ag mirror was used at the rear surface (ITO); hence, significant enhancements in  $J_{sc}$  and  $V_{oc}$  values were measured. The improvement in  $J_{sc}$  values can also be clearly seen in EQE curves [19].

In [25], instead of Ag mirror, Ag NPs were used together with Al<sub>2</sub>O<sub>3</sub> passivation layer. It is concluded in this study that using Ag NPs at rear surface enhanced the optical quality of the solar cell, and this can be seen through improved  $J_{sc}$  values and EQE curves. It is also concluded that this approach needs optimization because there should be a more homogeneous Ag NPs layer to help optical improvements.

### 3.4. Solar Simulator Results

In this sub-section, change in open circuit voltage ( $V_{oc}$ ), current density ( $J_{sc}$ ) and power conversion efficiency ( $\eta$ ) values of the CIGS solar cells, before and after the implementation of the passivation approaches, will be given in detail.

The  $V_{oc}$  and  $J_{sc}$ , and the efficiency values of the studies given in Table 1 with respect to the thickness of the absorber layer are indicated in Figures 3 and 4, for both reference and passivated devices.

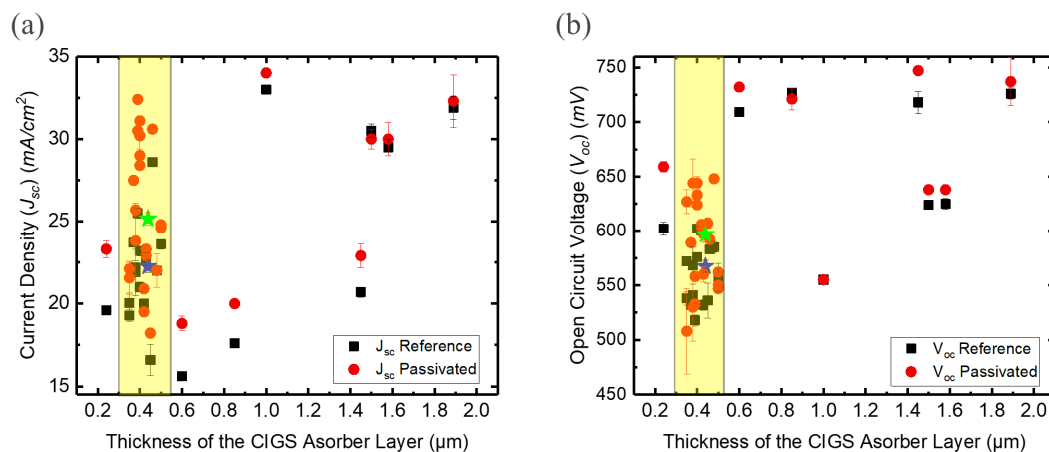


**Figure 3.** (a) Current density ( $J_{sc}$ ) and (b) open circuit voltage ( $V_{oc}$ ) values, before and after introducing the passivation layer, with respect to thickness of the absorber layer. The yellow boxes are given to guide the eye. The green and blue stars represent the average values of passivated and reference devices in the given interval, respectively.



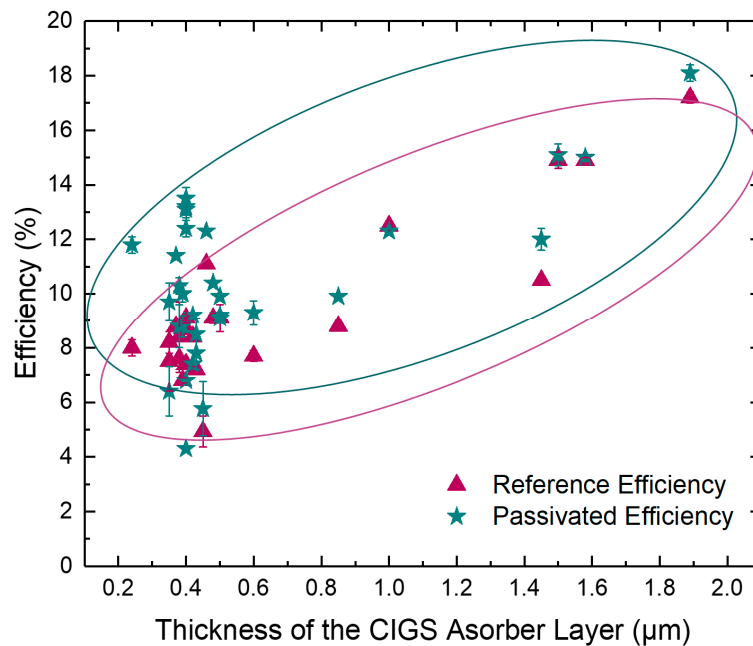


**Figure 4.** Average power conversion efficiency (%) of CIGS solar cells with respect to thickness of the absorber layer before and after the addition of passivation layer. The green and purple ovals are given to guide the eye.

For thick CIGS absorber layers ( $>800$  nm), except for one study [24], the  $V_{oc}$  was enhanced for all studies after the implementation of the passivation layer. For  $J_{sc}$  on the other hand, there were slight differences between reference and passivated devices for thick absorber layers (Figure 3).

For the thickest CIGS absorber layer, i.e.,  $1.89 \mu\text{m}$ , the difference between passivated and reference devices are hardly noticeable for  $V_{oc}$  and  $J_{sc}$ , but there is still an improvement [16]. On the other hand, for the thinnest CIGS absorber layer, i.e.,  $240$  nm, there are clear improvements in both  $V_{oc}$  and  $J_{sc}$ , as expected [18].

The effects of the passivation mechanism are more observable for thinner CIGS absorber layers, as explained earlier. In order to address these effects, there are two yellow boxes in Figure 3. These boxes point out the interval between  $0.3 \mu\text{m}$  and  $0.5 \mu\text{m}$ . To make the outcomes of the studies in this interval clearer, the average of the  $V_{oc}$  and  $J_{sc}$  of the reference and passivated devices is given with the star icons. The green stars belong to the passivated devices and the blue stars belong to the reference devices (Figure 3).

According to the difference between blue (reference) and green (passivated) star icons in Figure 3a, introducing the passivation layer boosted the  $J_{sc}$  for thin/ultra-thin CIGS solar cells. Displayed as blue (reference) and green (passivated) star icons in Figure 3b, the gain in  $V_{oc}$  can easily be observed for thin and ultra-thin CIGS solar cells. There are few outliers in the graphs that can be discussed. The first one is [17]. In this study, for the device which has a  $600$  nm thick absorber layer, they used low In and flat Ga. Hence, the  $J_{sc}$  is low for both the reference and the passivated device ( $\sim 15$  mA/cm<sup>2</sup> and  $\sim 18$  mA/cm<sup>2</sup>, respectively). Although the  $J_{sc}$  was improved significantly after the implementation of the passivation layer, it was still lower than almost all of the other studies given in Table 1. The second outlier we want to discuss is [24], which used a  $1 \mu\text{m}$  CIGS absorber layer. In this study, the  $V_{oc}$  values before and after the addition of the passivation layer were slightly lower than other studies that had thicker absorber layers, due to the lack of Na. In [24], for the reference sample, there was not an additional Na supply to enhance  $V_{oc}$ . For the passivated device, additional Na supply and Al<sub>2</sub>O<sub>3</sub> as a passivation layer were not sufficient to enhance  $V_{oc}$  (Figure 3b). On the contrary, they were sufficient enough to enhance the  $J_{sc}$  (Figure 3a).

After examining Figure 3, it can be concluded that after introducing a passivation layer with point contact openings, the electrical and/or optical properties of the CIGS solar cells were improved. The quality of the solar cells can be determined by  $FF$ . After adding the passivation layer, a good  $FF$  indicates that the contacting area is well-defined. However, a low  $FF$  shows the need for optimization in the passivation layer [9].  $FF$  was positively affected for nearly all the studies given in Table 1. For few studies, like [15], it was decreased due to the increase in series resistance and shunt conductance.

The effect of the passivation layer on the efficiency of both conventional and ultra-thin CIGS solar cells is given in Figure 4. Figure 4 indicates the efficiency of the passivated and reference CIGS solar cells with respect to the thickness of the absorber layer for all the studies given in Table 1.

After the addition of the passivation layer with point contact openings, the power conversion efficiencies of both conventional and ultrathin CIGS solar cells were increased in nearly all studies given in Table 1. However, considering Figure 4, the difference between passivated and un-passivated cells becomes apparent for the thinner (<800 nm) cells. It is seen that for some cases the power conversion efficiency of ultrathin CIGS solar cells reached up to 14% after the addition of the passivation layer. This value is nearly equal to the average power conversion efficiency of conventional unpassivated CIGS solar cells (Figure 4).

It is a well-known fact that the efficiency values of ultra-thin CIGS solar cells are still way too low from the record efficiency of conventional CIGS solar cell. However, the aforementioned studies have proven that the addition of the passivation layer on the rear contact is a promising technique to achieve higher values, i.e., record efficiencies.

### 3.5. Other Characterization Techniques for Further Characterizations

In order to examine the effect of the passivation layer, photoluminescence (PL) and external quantum efficiency (EQE) measurements were done besides solar simulator measurements.

PL is often used to reach a qualitative conclusion of the effect of the passivation layer, especially the influence of both radiative and non-radiative defects [9]. Under the influence of non-radiative recombination, the PL yield decreases [5]. CIGS solar cells that have a passivation layer have a narrower PL curve and/or higher PL intensity than reference/un-passivated solar cells. In [9], according to the authors, the smaller peak width of the PL response from the  $Al_2O_3$  passivated solar cells can be used as proof that the  $Al_2O_3$  layer was passivating the rear surface of CIGS solar cells.

Rear surface passivation leads to an increase in  $V_{oc}$ , as explained earlier, and  $J_{sc}$  due to an increase in rear internal reflection (Rb). EQE measurement is another commonly used technique to prove the improvements in the carrier collection of the passivated cells compared with reference/un-passivated cells [14]. The effect of the passivation layer on EQE is more significant for ultra-thin CIGS solar cells due to the unabsorbed photons that get a second chance to be absorbed after being reflected back into the absorber layer. For thicker samples, where all photons are absorbed after one pass in the absorber layer, the increase in EQE can be explained by a longer minority carrier diffusion length and/or a large space charge region, which makes it possible to collect the additional generated carriers in back of the thick samples [17].

## 4. Conclusions

After the realization of the importance and positive effects of implementation of the passivation layer at rear contact for both conventional and ultra-thin CIGS solar cells, nearly thirty studies were published which only focus on the rear surface passivation of CIGS solar cells.

To conclude, remarkable progress has been made in creating dielectric-based rear contact passivation strategies for CIGS solar cells. A cell efficiency of 18.1% has been achieved with the conventional, i.e., 1.89  $\mu m$  thick absorber layer, CIGS solar cell which has a 5 nm thick atomic-layer-deposited  $Al_2O_3$  passivation layer with contact openings realized with photo-lithography [16]. For ultra-thin, i.e., 0.4  $\mu m$  thick absorber layer, CIGS solar cells, the highest efficiency value, 13.5%, was realized in [14]. In this study, a 5 nm thick atomic-layer-deposited  $Al_2O_3$

passivation layer was used in combination with a 100 nm thick MgF<sub>2</sub> layer. There are some techniques, like CBD of CdS NPs, ALD of Al<sub>2</sub>O<sub>3</sub> etc., which were used as a proof of concept but can still be optimized and resulted in enhanced electrical and optical characteristics of the CIGS solar cells but with  $V_{oc}$  still far below the results for thick CIGS solar cells. The highest  $V_{oc}$  for thin CIGS was achieved for lithography [17]. However, additional Na has a considerable effect on  $V_{oc}$ , and it is not always easy to reveal the effect of passivation layer alone. Nevertheless, there are still a lot of approaches that need optimization like using very thin passivation layers to allow tunneling or using different oxides, such as TiO<sub>x</sub>, HfO<sub>x</sub>, etc., as a passivation layer [31,32]. Furthermore, passivation layers combined with light management techniques, like using Ag NP metallic mirrors below the passivation layers, require some improvements. In the near future, undoubtedly, most of these approaches will be optimized and many other approaches will be invented. From an industrial point of view, producing a highly efficient, low-cost CIGS solar cell is important to meet the need of building integrated photovoltaic technology (BIPV). Using the abovementioned approaches to passivate the rear surface of the CIGS solar cells, i.e., to increase the power conversion efficiency, it is more likely to increase the demand of the CIGS solar cells in industry.

**Author Contributions:** Conceptualization, G.B. and B.V.; Formal Analysis, G.B.; Investigation, G.B.; Writing—Original Draft Preparation, G.B.; Writing—Review & Editing, G.B., J.d.W. and B.V.; Visualization, G.B.; Supervision, B.V. and J.d.W.; Project Administration, M.M. and J.P.; Funding Acquisition, B.V.

**Funding:** This work received funding from the European Union’s H2020 research and innovation program under grant agreement No. 715027.

**Conflicts of Interest:** The authors declare no conflict of interest.

## References

1. Fraunhofer Institute for Solar Energy Systems, Photovoltaics Report. 2018. Available online: <https://www.ise.fraunhofer.de/content/dam/ise/de/documents/publications/studies/Photovoltaics-Report.pdf> (accessed on 16 December 2018).
2. Reinhard, P.; Chirilă, A.; Blösch, P.; Pianezzi, F.; Nishiwaki, S.; Buecheler, S. Review of progress toward 20% efficiency flexible cigs solar cells and manufacturing issues of solar modules. *IEEE J. Photovolt.* **2013**, *3*, 572–580. [[CrossRef](#)]
3. Green, M.A.; Hishikawa, Y.; Dunlop, E.D.; Levi, D.H.; Hohl-Ebinger, J.; Ho-Baillie, A.W.Y. Solar cell efficiency tables (version 52). *Prog. Photovolt. Res. Appl.* **2018**, *26*, 427–436. [[CrossRef](#)]
4. Feurer, T.; Reinhard, P.; Avancini, E.; Bissig, B.; Löckinger, J.; Fuchs, P.; Carron, R.; Weiss, T.P.; Perrenoud, J.; Stutterheim, S.; et al. Progress in thin film CIGS photovoltaics—Research and development, manufacturing, and applications. *Prog. Photovolt. Res. Appl.* **2017**, *25*, 645–667. [[CrossRef](#)]
5. Mollica, F.; Goffard, J.; Jubailt, M.; Donsanti, F.; Collin, S.; Cattoni, A.; Lombez, L.; Naghavi, N. Comparative study of patterned TiO<sub>2</sub> and Al<sub>2</sub>O<sub>3</sub> layers as passivated back-contact for ultra-thin Cu(In, Ga)Se<sub>2</sub> solar cells. In Proceedings of the 2016 IEEE 43rd Photovoltaic Specialists Conference (PVSC), Portland, OR, USA, 5–10 June 2016; pp. 2213–2217.
6. Lundberg, O.; Edoff, M.; Stolt, L. The effect of Ga-grading in CIGS thin film solar cells. *Thin Solid Films* **2005**, *480–481*, 520–525. [[CrossRef](#)]
7. Mollica, F. Optimization of Ultra-Thin Cu(In,Ga)Se<sub>2</sub> Based Solar Cells With Alternative Back-Contacts. Ph.D. Thesis, Université Pierre et Marie Curie, Paris, France, June 2017.
8. Dingemans, G.; Kessels, W.M.M. Status and prospects of Al<sub>2</sub>O<sub>3</sub>—Based surface passivation schemes for silicon solar cells. *J. Vac. Sci. Technol.* **2012**, *30*, 040802. [[CrossRef](#)]
9. Salomé, P.M.P.; Vermang, B.; Ribeiro-Andrade, R.; Teixeira, J.P.; Cunha, J.M.V.; Mendes, M.L.; Haque, S.; Borme, J.; Águas, H.; Fortunato, E.; et al. Passivation of interfaces in thin film solar cells: Understanding the effects of a nanostructured rear point contact layer. *Adv. Mater. Interfaces* **2018**, *5*, 1701101. [[CrossRef](#)]
10. Joel, J. Characterization of Al<sub>2</sub>O<sub>3</sub> as CIGS Surface Passivation Layer in High-Efficiency CIGS Solar Cells. Ph.D. Thesis, Uppsala Universitet, Uppsala, Sweden, July 2014.

11. Casper, P.; Hünig, R.; Gomard, G.; Kiowski, O.; Reitz, C.; Lemmer, U.; Powalla, M.; Hetterich, M. Optoelectrical improvement of ultra-thin Cu(In,Ga)Se<sub>2</sub> solar cells through microstructured MgF<sub>2</sub> and Al<sub>2</sub>O<sub>3</sub> back contact passivation layer. *Phys. Status Solidi RRL* **2016**, *10*, 376–380. [[CrossRef](#)]
12. Vermang, B.; Fjällström, V.; Pettersson, J.; Salomé, P.; Edoff, M. Development of rear surface passivated Cu(In,Ga)Se<sub>2</sub> thin film solar cells with nano-sized local rear point contact. *Sol. Energy Mater. Sol. Cells* **2013**, *117*, 505–511. [[CrossRef](#)]
13. Vermang, B.; Fjällström, V.; Gao, X.; Edoff, M. Improved Rear Surface Passivation of Cu(In,Ga)Se<sub>2</sub> Solar Cells: A Combination of an Al<sub>2</sub>O<sub>3</sub> Rear Surface Passivation Layer and Nanosized Local Rear Point Contacts. *IEEE J. Photovolt.* **2014**, *4*, 486–492. [[CrossRef](#)]
14. Vermang, B.; Wätjen, J.T.; Fjällström, V.; Rostvall, F.; Edoff, M.; Kotipalli, R.; Henry, F.; Flandre, D. Employing Si solar cell technology to increase efficiency of ultra-thin Cu(In,Ga)Se<sub>2</sub> solar cells. *Prog. Photovolt. Res. Appl.* **2014**, *22*, 1023–1029. [[CrossRef](#)]
15. Vermang, B.; Wätjen, J.T.; Fjällström, V.; Rostvall, F.; Edoff, M.; Kotipalli, R.; Henry, F.; Flandre, D. Highly reflective rear surface passivation design for ultra-thin Cu(In,Ga)Se<sub>2</sub> solar cells. *Thin Solid Films* **2015**, *582*, 300–303. [[CrossRef](#)]
16. Choi, S.; Kamikawa, Y.; Nishinaga, J.; Yamada, A.; Shibata, H.; Niki, S. Lithographic fabrication of point contact with Al<sub>2</sub>O<sub>3</sub> rear-surface-passivated and ultra-thin Cu(In,Ga)Se<sub>2</sub> solar cells. *Thin Solid Films* **2018**, *665*, 91–95. [[CrossRef](#)]
17. Ledinek, D.; Salomé, P.; Hagglund, C.; Zimmermann, U.; Edoff, M. Rear Contact Passivation for High Bandgap Cu(In, Ga)Se<sub>2</sub> Solar Cells with a Flat Ga profile. *IEEE J. Photovolt.* **2018**, *8*, 1–7. [[CrossRef](#)]
18. Vermang, B.; Wätjen, J.T.; Frisk, C.; Fjällström, V.; Rostvall, F.; Edoff, M.; Salomé, P.; Borme, J.; Nicoara, N. Introduction of Si PERC rear contacting design to boost efficiency of Cu(In,Ga)Se<sub>2</sub> solar cells. *IEEE J. Photovolt.* **2014**, *4*, 1644–1649. [[CrossRef](#)]
19. Yin, G.; Knight, M.W.; Lare, M.-C.v.; Garcia, M.M.S.; Polman, A.; Schmid, M. Optoelectronic Enhancement of Ultrathin CuIn<sub>1-x</sub>Ga<sub>x</sub>Se<sub>2</sub> Solar Cells by Nanophotonic Contacts. *Adv. Opt. Mater.* **2017**, *5*, 1–11.
20. Lare, M.-C.v.; Yin, G.; Polman, A.; Schmid, M. Light coupling and trapping in ultrathin Cu(In,Ga)Se<sub>2</sub> solar cells using dielectric scattering patterns. *ACS Nano* **2015**, *9*, 9603–9613. [[CrossRef](#)] [[PubMed](#)]
21. Vermang, B.; Rostvall, F.; Fjällström, V.; Edoff, M. Potential-induced optimization of ultra-thin rear surface passivated CIGS solar cells. *Phys. Status Solidi RRL* **2014**, *8*, 908–911. [[CrossRef](#)]
22. Yin, G.; Knight, M.W.; Lare, M.-C.v.; Garcia, M.M.S.; Polman, A.; Schmid, M. Well-Controlled Dielectric Nanomeshes by Colloidal Nanosphere Lithography for Optoelectronic Enhancement of Ultrathin Cu(In,Ga)Se<sub>2</sub> Solar Cells. *ACS Appl. Mater. Interfaces* **2016**, *8*, 31646–31652. [[CrossRef](#)]
23. Bose, S.; Cunha, J.M.V.; Suresh, S.; Wild, J.D.; Lopes, T.S.; Barbosa, J.R.S.; Silva, R.; Borme, J.; Fernanaes, P.A.; Vermang, B.; et al. Optical Lithography Patterning of SiO<sub>2</sub> Layers for Interface Passivation of Thin Film Solar Cells. *Sol. RRL* **2018**, *2*, 1800212. [[CrossRef](#)]
24. Ledinek, D.; Donzel-Gargand, O.; Sköld, M.; Keller, J.; Edoff, M. Effect of different Na supply methods on thin Cu(In,Ga)Se<sub>2</sub> solar cells with Al<sub>2</sub>O<sub>3</sub> rear passivation layers. *Sol. Energy Mater. Sol. Cells* **2018**, *187*, 160–169. [[CrossRef](#)]
25. Suresh, S.; Wild, J.D.; Kohl, T.; Buldu, D.G.; Brammertz, G.; Meuris, M.; Poortmans, J.; Isabella, O.; Zeman, M.; Vermang, B. A study to improve light confinement and rear-surface passivation in a thin Cu(In,Ga)Se<sub>2</sub> solar cell. *Thin Solid Films* **2018**, *669*, 399–403. [[CrossRef](#)]
26. Vermang, B.; Goverde, H.; Tous, L.; Lorenz, A.; Choulart, P.; Horzel, J.; John, J.; Poortmans, J.; Mertens, R. Approach for Al<sub>2</sub>O<sub>3</sub> rear surface passivation of industrial p-type Si PERC above 19%. *Prog. Photovolt. Res. Appl.* **2012**, *20*, 269–273. [[CrossRef](#)]
27. Kotipalli, R.; Vermang, B.; Joel, J.; Rajkumar, R.; Edoff, M.; Flandre, D. Investigating the electronic properties of Al<sub>2</sub>O<sub>3</sub>/Cu(In,Ga)Se<sub>2</sub> interface. *AIP Adv.* **2015**, *5*, 107101. [[CrossRef](#)]
28. Keller, J.; Chen, W.-C.; Riekehr, L.; Kubart, T.; Törndahl, T.; Edoff, M. Bifacial Cu(In,Ga)Se<sub>2</sub> solar cells using hydrogen-doped In<sub>2</sub>O<sub>3</sub> films as a transparent back contact. *Prog. Photovolt. Res. Appl.* **2018**, *26*, 846–858. [[CrossRef](#)]

Using hydrogen-doped In<sub>2</sub>O<sub>3</sub> films as a transparent back contact in (Ag,Cu)(In,Ga)Se<sub>2</sub> solar cells. *Prog. Photovolt. Res. Appl.* **2018**, *26*, 159–170. [[CrossRef](#)]

29. Ohm, W.; Riedel, W.; Aksünger, U.; Greiner, D.; Kaufmann, C.A.; Lux-Steiner, M.C.; Gledhill, S. Bifacial Cu(In,Ga)Se<sub>2</sub> solar cells with submicron absorber thickness: Back-contact passivation and light management. In Proceedings of the 2015 IEEE 42nd Photovoltaic Specialist Conference (PVSC), New Orleans, LA, USA, 14–19 June 2015; pp. 1–5.
30. Edoff, M.; Joel, J.; Vermang, B.; Hagglund, C. Back contact passivation effects in Bi-facial thin CIGS solar cells. In Proceedings of the 2016 IEEE 43rd Photovoltaic Specialists Conference (PVSC), Portland, OR, USA, 5–10 June 2016; pp. 3527–3530.
31. Titova, V.; Veith-Wolf, B.; Startsev, D.; Schmidt, J. Effective passivation of crystalline silicon surfaces by ultrathin atomic-layer-deposited TiO<sub>x</sub> layers. *Energy Procedia* **2017**, *124*, 441–447. [[CrossRef](#)]
32. Zhang, X.-Y.; Hsu, C.-H.; Lien, S.-Y.; Chen, S.-Y.; Huang, W.; Yang, C.-H.; Kung, C.-Y.; Zhu, W.-Z.; Xiong, F.-B.; Meng, X.-G. Surface passivation of silicon using hfo<sub>2</sub> thin films deposited by remote plasma atomic layer deposition system. *Nanoscale Res. Lett.* **2017**, *12*, 324. [[CrossRef](#)] [[PubMed](#)]



© 2019 by the authors. Licensee MDPI, Basel, Switzerland. This article is an open access article distributed under the terms and conditions of the Creative Commons Attribution (CC BY) license (<http://creativecommons.org/licenses/by/4.0/>).